Sensitivity of ground magnetometer array elements for GIC applications I: Resolving spatial scales with the BEAR and CARISMA arrays

Stavros Dimitrakoudis [1], David K. Milling [1], Andy Kale [1], Ian R. Mann [1]

[1]Department of Physics, University of Alberta, Edmonton, Alberta, Canada

Key Points:

- Occurrence distributions of dB_H/dt during two similar storms at two different ground magnetometer arrays are found to be log-normal
- Two-point dB_H/dt vector correlations between distant stations are lower within the auroral oval than at mid-latitudes
- Magnetometers placed 200 km apart should provide required coverage of localized large dB_H/dt events for GIC applications

Corresponding author: Stavros Dimitrakoudis, `dimitrak@ualberta.ca`

Abstract

Geomagnetically induced currents (GICs) can be driven in terrestrial electrical power grids as a result of the induced electric fields arising from geomagnetic disturbances (GMD) resulting from the dynamics of the coupled magnetosphere-ionosphere-ground system. However, a key issue is to assess an optimum spacing for the magnetometer stations in order to provide appropriate monitoring of the GIC-related GMD. Here we assess the vector correlation lengths of GMD and related amplitude occurrence distribution of the variations of horizontal magnetic field dB_H/dt. Specifically, we study the GMD response to two storm-time substorms using data from two magnetometer arrays, the Baltic Electromagnetic Array Research (BEAR) Project in Scandinavia and the Canadian Array for Realtime Investigations of Magnetic Activity (CARISMA) array in North America, so as to determine the optimal magnetometer spacing in latitude and longitude, for monitoring and assessing GIC risk. We find that although magnetic disturbances are well-correlated up to distances of several hundred kilometers at mid-latitudes, the vector correlation length rapidly drops off for station separations of less than 100 km within the auroral oval. In general geomagnetic fluctuations are stronger and more localized in the auroral zone. Since the auroral oval is pushed equatorward during intense magnetic storms, we highlight that networks using a station separation of $\sim$ 200 km should provide an excellent basis for monitoring both small and large scale geomagnetic disturbances. A monitoring network with this station spacing is recommended as being optimal for assessing the role of GMD in driving GICs in the electric power grid.

Plain Language Summary

One of the most dangerous effects of space weather is the induction of currents on wires and pipelines on Earth, which can destroy electrical transformers in the power grid and damage infrastructure. Part of our effort to deal with that threat involves monitoring the variability of the Earth's magnetic field at the Earth's surface, since that can give us an indication of how and when such currents may be induced. A key issue is the required spatial separations of observing magnetic monitoring stations. Using two existing arrays of ground stations we statistically analyzed their observations during two days of strong space-related geomagnetic activity. From that analysis we have found that regions in the auroral zone have intense and more localized geomagnetic variations, compared to regions equatorward of them. Since the auroral zone can be pushed equator-

ward at times of intense geomagnetic storms, which is when the induced currents will likely pose the greatest risk, we need to account for separations which can additionally monitor small-scale fluctuations. We conclude that arrays of ground magnetometers with a ~ 200 km separation are optimum for the required magnetic monitoring.

1 Introduction

Geomagnetic disturbances (GMD) due to space weather are well-known to pose a major threat to terrestrial electric power distribution systems through the generation of Geomagnetically Induced Currents (GIC) in power transmission lines (e.g., Lanzerotti, 1979; Boteler et al., 1998). During a large GMD, the GIC flow in transformers may cause half-cycle saturation, which can increase absorption of reactive power, generate harmonic currents, and cause transformer hot spot heating and potential failure (e.g., Molinski, 2002). Increased transformer reactive power absorption and harmonic currents associated with GMD events can also cause protection system misoperation and loss of reactive power sources, the combination of which can lead to voltage collapse(e.g., NERC, 2012).

Accurate modelling of the GIC produced during space weather events requires the inclusion of the appropriate power system characteristics, magnetic source fields and Earth conductivity structure (e.g., Boteler & Pirjola, 2017). The important aspects of the magnetic source fields are the amplitude, polarisation, frequency content and spatial characteristics of the disturbance. Different physical mechanisms produce disturbances with different spatial and temporal features (e.g,. Viljanen, 2012). For instance, the ring current generated during the magnetic storm main phase produces disturbances on a global scale which may be considered to be fairly uniform. In contrast, the magnetic disturbances observed during auroral substorms are due to a combination of field-aligned currents in the magnetosphere and electrojet currents in the ionosphere at a height of $\sim$ 100 km above the Earth's surface which lead to more localized and complex disturbance fields (Viljanen et al., 2006; Huttunen et al., 2008). For a discussion of some of the drivers of storm-time magnetic disturbances in the magnetosphere and their connection to variations of the horizontal magnetic field at the surface of the Earth, see for example Kataoka and Pulkkinen (2008) and references therein.

In view of the long-term risk posed by GICs to infrastructure, the United States' Federal Energy Regulatory Commission has approved Reliability Standard TPL-007-1, which establishes the requirement for power companies to assess the vulnerability of their transmission systems according to specified guidelines (United States of America Federal Energy Regulatory Commission, 2016). The potential of GMDs to produce GICs is to be evaluated using spatially-averaged data in 500 km x 500 km regions, based on the observational results of Pulkkinen et al. (2015) and on theoretical considerations of the spatial structure of the large-scale auroral electrojet (Pulkkinen et al., 2006). However, the Commission also proposed that further studies be undertaken for possible modifications of the benchmark GMD event definition, which is based on that spatially-averaging convention. In this paper we explore the evolution and statistics of dB/dt, a GIC proxy (e.g., Heyns et al., 2021, and references therein), over the course of two magnetic storms in two magnetometer arrays, the dense Baltic Electromagnetic Array Research (BEAR, a part of EUROPROBE's SVEKALAPKO project (Hjelt & Daly, 1996)) and the sparser but wider Canadian Array for Realtime InvestigationS of Magnetic Activity (CARISMA) (Mann et al., 2008).

In a manner similar to the analysis of Viljanen et al. (2001) we analyse the occurrence distributions of the time variations of the horizontal magnetic disturbance at the Earth's surface on a range of timescale. We further assess in detail the vector spatial correlation of such disturbances to assess the optimum and/or recommended spacing between magnetometer stations which should be deployed in arrays designed to provide continuous monitoring of GMD for applications assessing the space weather risk, for example, to electric power grids arising from the resulting GICs.

2 Data Processing

Since the rate of change of the horizontal component of $d\mathbf{B}/dt$ on the ground correlates with GICs (Coles et al., 1992; Mäkinen, 1992; Viljanen, 1998; Bolduc et al., 1998), we use that as a proxy. Although it is sometimes calculated as $dB_H/dt = d\sqrt{B_x^2 + B_y^2}/dt$ (e.g. Thomson et al., 2011; Rodger et al., 2017), we find that such an approach makes the results dependent on baseline subtractions while also being insensitive to rotations of $\mathbf{B_H}$. To avoid these two issues, and since we are interested in the electric field which may produce directional electric fields which drive GICs in one-dimensional electric power lines, we instead calculate it as $dB_H/dt = \sqrt{(dB_x/dt)^2 + (dB_y/dt)^2}$ (Viljanen et al.,

2001). Values of $dB_H/dt > 1$nT/s are considered noteworthy (Viljanen et al., 2001), although their total effect may be cumulative with time, and the generation of significant voltage differences along a given power line infrastructure also additionally depends on the spatial structure of the driving fields along the line (see (Marshall et al., 2010) for discussion on a GIC index). We followed two approaches for evaluating the statistical properties of dB_H/dt. First, we analysed the response of a very dense magnetometer array, BEAR, in a single day of high geomagnetic activity; then we analysed the response of a sparser array, CARISMA, in a day of very similar geomagnetic activity. The two approaches are complementary.

The Baltic Electromagnetic Array Research (BEAR) array operated between June and July 1998, with a total of 75 stations scattered across Norway, Sweden, Finland, Estonia, and the Russian Federation. The condition $dB_H/dt > 1$nT/s is met infrequently in the course of the BEAR measurements. A single day, 26 June 1998, stands out with 84600 such occurrences concentrated within a four-hour time period that corresponds to high Kp and increasingly negative Dst. Therefore, we focused on that one day exclusively in our analysis of BEAR data. In this study we have only made use of BEAR stations that provided full coverage during our selected time intervals, with a sampling rate of 2s and no instrumental irregularities. This limited our coverage to the 42 stations shown in Figure 1. To test for longitudinal or latitudinal dependencies on the spatial scale, we subsequently considered subsets of those stations lying along the lines of magnetic latitudes 56.5° N, 61° N and 63.5° N, as well as magnetic longitude 105° E. Furthermore, we distinguished between stations north or south of the 59.5° N line. These groups are denoted with boxes (diamonds and squares) of their own specific colors in Figure 1, the same colours being used in all subsequent figures that use their measurements.

The Canadian Array for Realtime InvestigationS of Magnetic Activity (CARISMA) has been in operation since 2005, succeeding the previous Canadian Auroral Network for the OPEN Program Unified Study (CANOPUS) array (Mann et al., 2008). Out of numerous substorm periods that have occurred since then, we have identified one whose characteristics closely match those of the one observed with BEAR, on 7 January 2015. At that time, there were 19 operational CARISMA stations, which we could divide along certain lines of magnetic latitude or longitude, as shown in Figure 2. CARISMA's standard data product uses a sampling rate is 1s, which affords us higher temporal resolution than BEAR. While the shortest distance between stations is only 210 km, compared

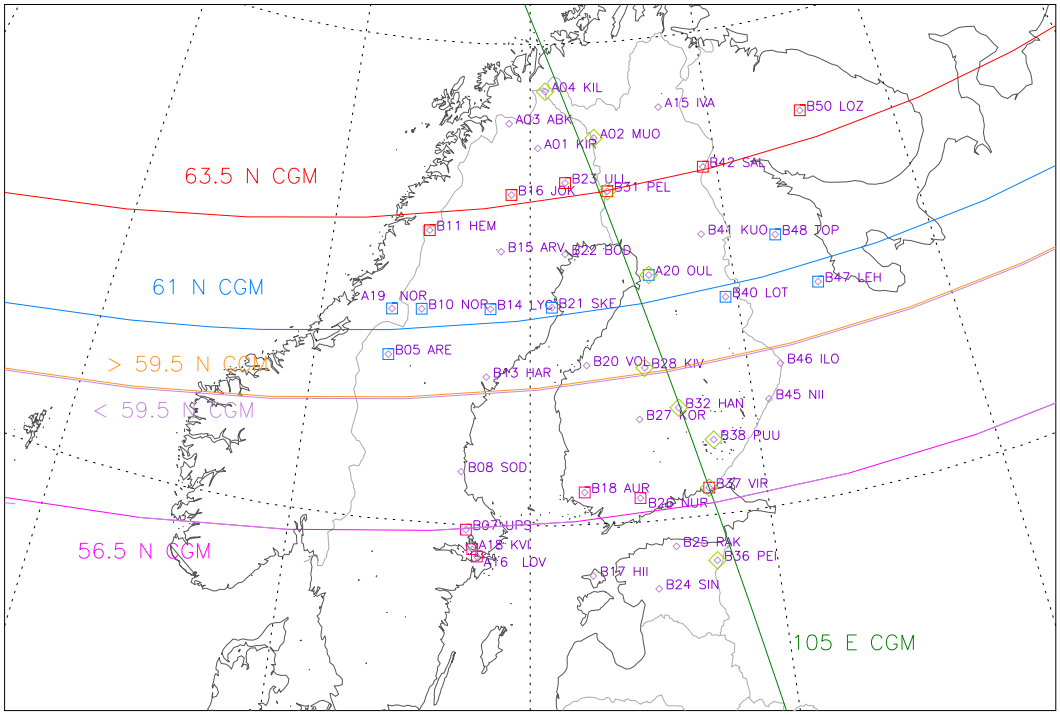

Figure 1. Map of the BEAR magnetometer network, with the stations active on June 26 1998. The orange line denotes the border between northern and southern stations used in this study. The other lines denote groups of stations along constant magnetic latitude or longitude. Boxes and diamonds of these colours for each station further indicate which subset each BEAR station belongs to.

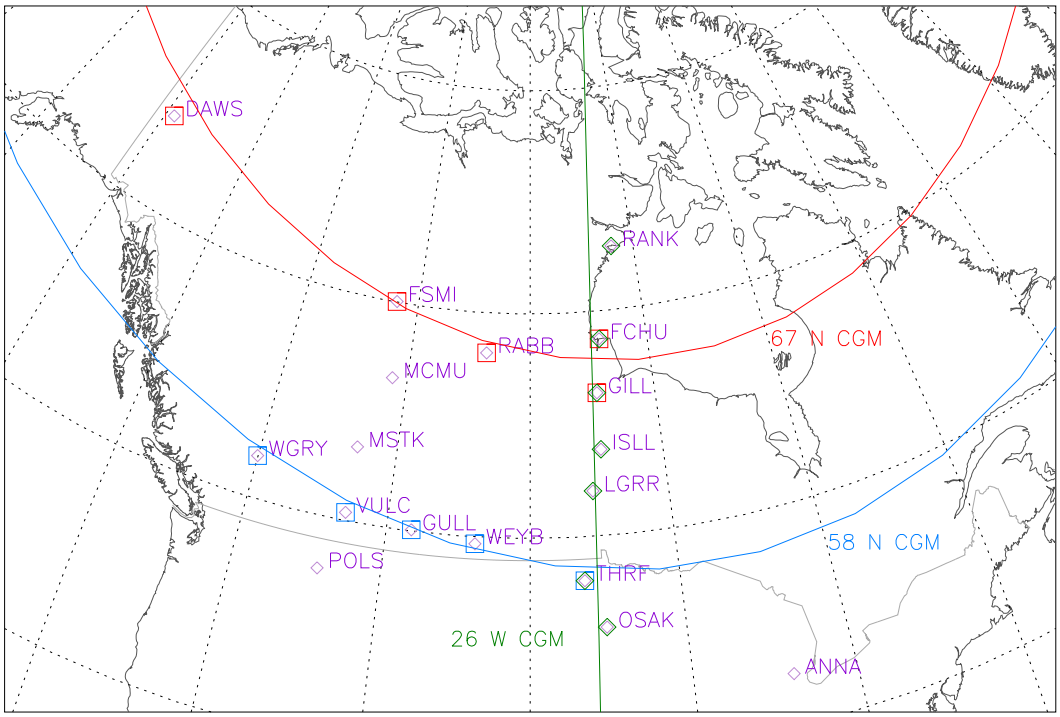

Figure 2. Map of the CARISMA stations active on January 7 2015. The red, blue, and green lines denote groups of stations along constant magnetic latitude or longitude. As in Figure 1, boxes and diamonds of these colours for each station further indicate which subset each CARISMA station belongs to.

to 20 km for BEAR, the longest distance is 3400 km, up from 1180 km for BEAR. Thus, the two arrays complement each other providing coverage of the structure of GMD across different spatial scales.

We also made use of SuperMAG (Gjerloev, 2009, 2012) in order to obtain polar maps of dB_H/dt vectors for the two events. Those maps also contain fitted magnetometer vectors that fill in the gaps between magnetometer stations (Waters et al., 2015). For the 26 June 1998 event they are juxtaposed on images of the auroral oval by the Visible Imaging System (VIS) (Frank et al., 1995), flown on the Polar Spacecraft. Kp and Dst values were extracted from NASA/GSFC's OMNI data set through OMNIWeb.

In order to evaluate the effect of ground distance on the coherence of dB_H/dt measurements, and thus also assess the accuracy of inferring the structure of GMD using measurements from magnetometers separated by various distances, we flagged each instance of $dB_{H_j}/dt > 1\text{nT/s}$ on a magnetometer j and then measured the concurrent dB_{H_i}/dt

on every other magnetometer i in the array or a subset of the array as needed. Under the conditions $dB_{H_i}/dt < dB_{H_j}/dt$ (to avoid double-counting) and $dB_{H_i}/dt > 0.5$nT/s (to avoid superfluous measurements), we obtained values of the vector correlation (under rotation) coefficient

$$\rho = \sqrt{\frac{(\sigma_{xu})^2 + (\sigma_{yv})^2 + (\sigma_{xv})^2 + (\sigma_{yu})^2}{\sigma_i^2 \sigma_j^2}}, \tag{1}$$

where the two components of dB_{H_i}/dt are designated with x and y, the two components of dB_{H_j}/dt are designated with u and v, and σ_i^2 and σ_{xu} are variances and covariances respectively (Hanson et al., 1992).

3 Results

Our case study for the BEAR magnetometer network is the substorm of 26 June 1998. Between 1:00 and 5:00 UTC Kp remains constant at 6+, while Dst drops to -101 nT, slowly recovering after 4:00 UTC (Figure 3). For the benefit of the reader, we plot the time series of the (magnetic north-south) H-component magnetometer time series from selected BEAR magnetometer stations is provided in Supplementary Material Figure S1. It is during this time period that the ground magnetometers in the BEAR array register a large number of strong dB_H/dt variations. Those, as we can tell by comparing the orange and purple dashed lines in Figure 3, predominantly occur in the northern region of the BEAR array; while there are 26 stations north of the arbitrarily chosen line of 59.5° N CGM compared to only 16 south of it, there are 82601 counts of $dB_H/dt >$ 1nT/s north of this line as compared to 1999 such counts south of it.

A more interesting picture emerges when we plot the occurrence distributions of the number of counts above certain dB_H/dt thresholds for each group of stations in Figure 4. These occurrence distributions appear to be log-normal, with their slopes clearly also dependent on latitude; those of the northern stations, and all stations in aggregate, follow the behaviour of the subset of stations along the 63.5° N line, those of southern stations closely match the subset of stations on the 56.5° N line, while stations along the 61 N line have an intermediate slope. That behaviour persists when we downsample our data to one minute cadence and assess the time rate of change of the horizontal magnetic field dervied from these 1 minute samples. However, note that the number of counts drops by more than the factor of 30 that we would expect in going from 2s to 60s data, indicating perhaps unsurprisingly that the short timescale rates of change more often

reach a specific threshold of nT/s than when derived from the longer period data. This is of course explained as a result of the fluctuating nature of the magnetic field disturbances. This result clearly shows that a one minute sampling rate underestimates the occurrence rate of such short timescale, high dB_H/dt events.

We can examine the dependence of the slope of the occurrence distributions as a function of latitude in greater detail by considering data from each individual station along the 105° E line (Figure 5). The gradients of these distributions, in log-linear space, increase gradually with latitude, except for a sharper and more localised jump at around 59.5° N, and which we used earlier to define a latitude separating stations in the northern and southern regions of the BEAR array. The gradient reaches a maximum at a latitude of around 65° N, above which there is a slight decrease. That latitude of the peak in the gradient of the occurrence distributions matches that of the latitudinal dependence of dB/dt amplitudes shown by Woodroffe et al. (2016). Indeed, previous studies have linked that maximum to the shifting location of the auroral oval as far back as (Coles & Boteler, 1993).

In order to further investigate the latitude dependence of the characteristics of the GMD, in Figure 6 we plot the means, quartiles, and upper values of dB_H/dt as a function of magnetic latitude for each station along the 105° E longitude line, calculated separately for data at three different sampling rates of 2s (raw; left panel (a)), 10s (middle panel, (b)), and 1 minute (right panel, (c)). In all three cases we see a steep increase in the characteristics of the distributions of the magnitude of dB_H/dtat at a latitude of around 60° N, especially for the highest recorded values (denoted upper value in Figure 6), and which predictably push the mean values above the medians. The one minute sampling rate data in panel (c) suffers somewhat from reduced count statistics, particularly at lower latitudes, and also indicates lower dB_H/dt changes in nT/s, since those would have to be sustained for a full minute to be recorded as the same amplitude as the 1s dB_H/dt magnitudes shown in panel (a). In Figure 7 we show polar maps of magnetic disturbance vectors from SuperMAG magnetometers at three times, in one-hour intervals, during the high dB_H/dt activity phase of the 26 June 1998 substorm. From concurrent VIS images of the auroral oval we can confirm that the large magnetic perturbations seen with SuperMAG and the large values of dB_H/dt seen with the BEAR array correspond to region of of the auroral oval over the European sector in the dawn local time sector.

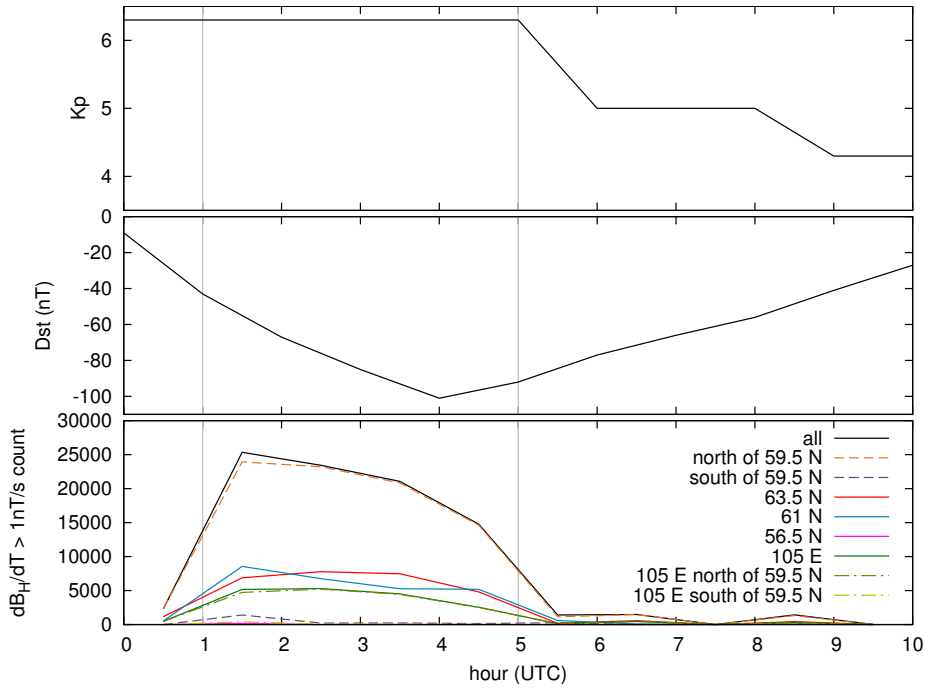

Figure 3. Kp, Dst, and dB_H/dt counts per hour, on 26 June 1998 with the BEAR array. Grey lines show the time span we used. Coloured lines correspond to data from different subsets of magnetometer stations, as shown in Figure 1.

In Figure 8 we show the values of the vector correlation ρ for the three constant-latitude groups of stations, for pairs of stations with stations in 50 km-wide bins, using BEAR magnetic data using both a two second (a) and one minute (b) sampling rate. Three important and clear trends are apparent. First, measurements at southern stations are spatially more well-correlated across larger longitudinal separations than those in the north. For example, this is particularly evident when comparing the magenta line, corresponding to 56.5° N, with the red line, corresponding to 63.5° N). Second, while the median values of $dB_{x,y_i}/dB_{x,y_j}$ drop roughly monotonically with station separation distance, the effect of a randomization of their angle θ after about 200 km means that their vector correlations drop precipitously from there at larger inter-station separations. Third, the one minute data shows very similar behaviour to the two second data, although to account for the lower count statistics we had to relax the $d\mathbf{B}_H/dt$ threshold which we used to collate the magnetic disturbances for this correlative assessment by a factor of ten.

To further investigate the effect of latitude on these inter-station vector correlations, we selected three stations along the 105 degrees E line, one at its southern tip, one

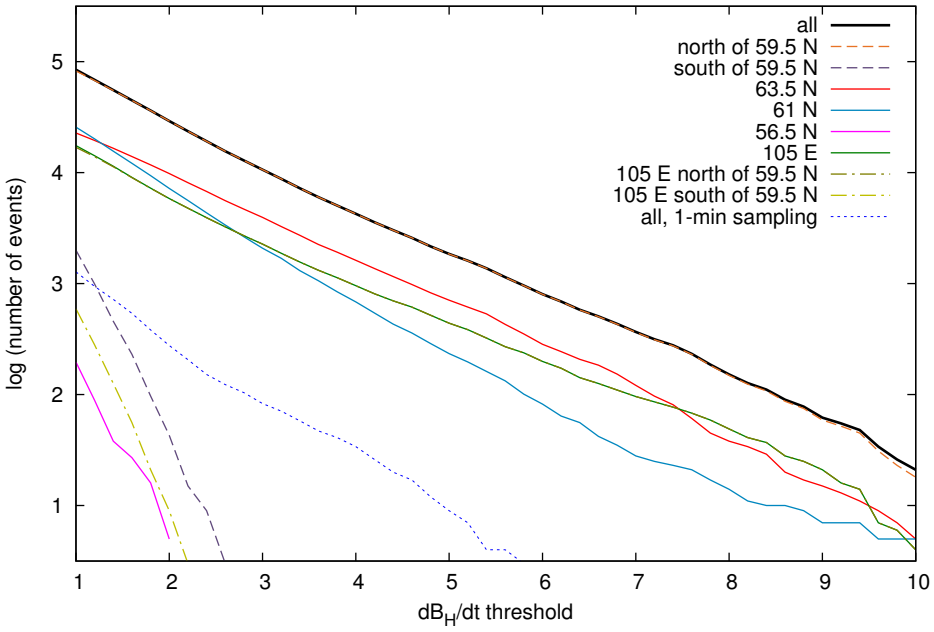

Figure 4. Occurrence distribution of dB_H/dt counts as a function of threshold, from 01:00 to 5:00 UTC on 26 June 1998, using 2s cadence data from the BEAR array. Coloured lines correspond to data derived from different subsets of stations, as shown in Figure 1. The short dashed lines show measurements derived from one minute cadence data for the same subsets of stations. See text for details.

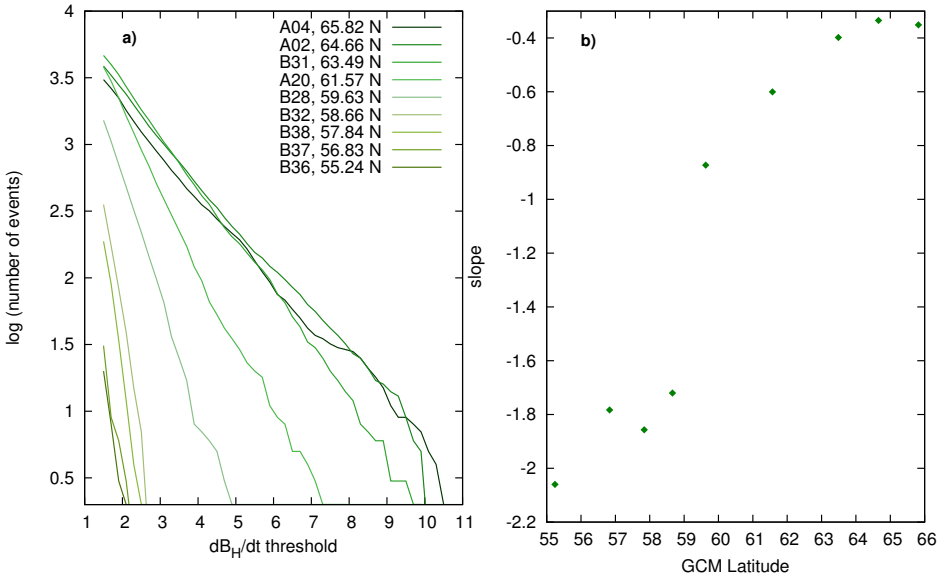

Figure 5. a) Occurrence distribution of dB_H/dt counts above a specific threshold (units nT/s), which occurred from from 01:00 to 5:00 UTC on 26 June 1998, for all individual stations along the 105° E (green) line of BEAR; b) Linear fits to the slopes of each logarithmic occurrence distribution line from panel (a) as a function of the latitude of the station.

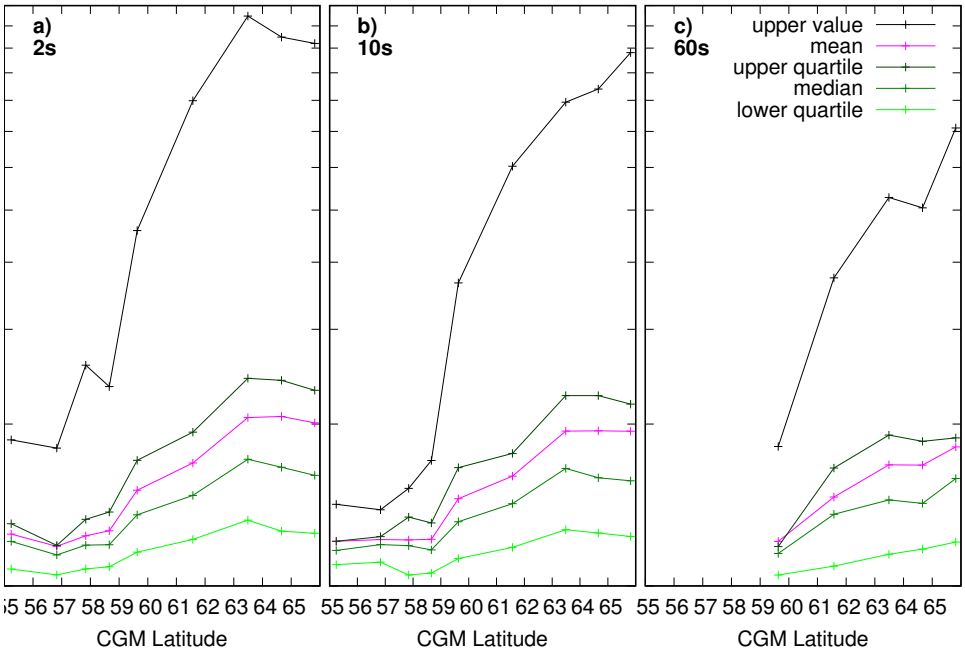

Figure 6. Mean, quartiles, and upper value of dB_H/dt measurements (for $dB_H/dt > 1$nT/s) taken from 01:00 to 5:00 UTC on 26 June 1998, for all stations along the 105° E (green) line of BEAR; with a) a two second sampling rate, b) a ten second sampling rate, and c) a one minute sampling rate.

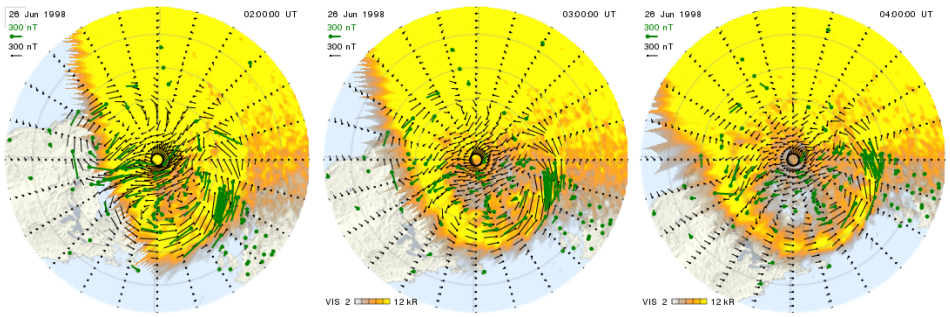

Figure 7. Polar maps from SuperMAG for the 26 June 1998 event, with Polar VIS images overlaid and which show the auroral oval. Three snapshots are shown, for 2:00 UTC, 3:00 UTC, and 4:00 UTC. A clear correspondance between the large magnetic perturbations and the auroral oval over the European sector, which is on the dawn flank at this time, is clear.

at its northern tip, and one in the middle, and calculated the two-point vector correlation of $d\mathbf{B}_H/dt$ between that station and all other stations along the same 105 degrees E line. The results are shown in Figure 9, which again shows clearly that the inter-station correlations drop as before with increasing distance, but they remain high for longer distances when using the lower latitude station as our point of reference. This further verifies the assertion that the correlation lengths as a function of latitude are longer at lower latitude locations. In our view, based for example on the correspondence between the Polar VIS images and the large SuperMAG fluctuations shown in Figure 7, it is likely that magnetic disturbances are influenced by variations in ionospheric conductivity. In the auroral zone, energetic electron precipitation and related changes in conductivity can lead to the generation of small scale conductance structures which are associated with large amplitude waves with small perpendicular scales, likely with polarisation rotations, perhaps amplified as a result of ionospheric feedback processes (cf. Lysak, 1991). Conversely, outside the auroral zone, the conductance at sub-auroral latitudes might be more spatially uniform leading to larger vector correlation lengths for GMD. It is also quite likely that there is also an impact from an amplitude selection effect as well. For example, as we saw in Figure 4, the number of $d\mathbf{B}_H/dt$ measurements above all thresholds increases almost monotonically with increasing latitude. Therefore, while the majority events captured at high latitudes, with typical amplitudes, will be associated with weaker and more uncorrelated measurements at low latitudes, any event strong enough to register at lower latitudes will most likely be related to similar and even larger measurements at higher latitudes. As a result the correlation length statistics at lower latitudes could be larger than those at higher latitudes as a result of the latitudinal dependence of the amplitudes of typical GMD.

The same latitudinal dependence of the inter-station vector correlation is also apparent when we reduce the data to a temporal cadence of one minute, although it should be noted that count statistics for the fixed amplitude threshold $d\mathbf{B}_H/dt$ are then very poor for the lowest latitude station, and all but the first three data points for it in panel (b) of Figure 9 correspond to fewer than ten pairings of measurements. The median angles of the individual $d\mathbf{B}_H/dt$ vectors also display some further differences as a function of latitude between the more northern and southern stations in the BEAR array, as shown in Figure 10. For the more southerly stations, variations predominantly occur with a polarisation in the East-West direction (panels (c, f, i)). For the more northerly stations

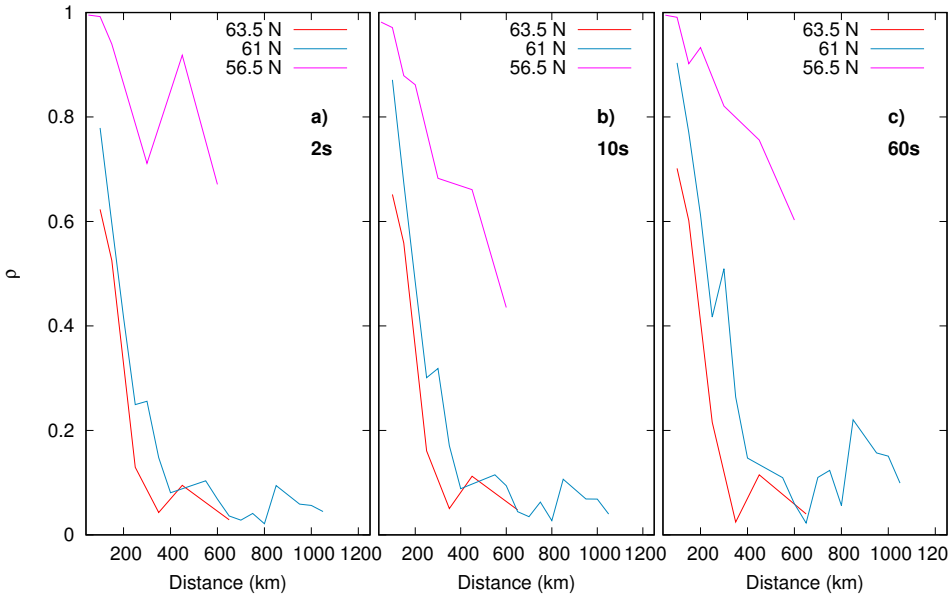

Figure 8. Vector correlation coefficients of concurrent dB_H/dt vectors from two different stations as a function of inter-station separation distances, between 1:00 and 5:00 UTC for the BEAR array; using a) a two second sampling rate, b) a ten second sampling rate, and c) a one minute sampling rate. Coloured lines correspond to different subsets of stations at constant latitude, as shown in Figure 1.

(panels (b, e, g), on the other hand, they are much more likely to occur in the North-South direction. Nonetheless, in all panels there is a significant variability in the direction of polarisation, with significant amplitudes occurring in almost all polarisation directions.

For CARISMA, we chose the substorm of 7 January 2015 as our comparator case study. Similar to the BEAR event, Kp retains a value of 6+ for three hours, only dropping to 4 at the tail end of our period of dB_H/dt measurements. Dst drops to -99 nT during the period of the largest dB_H/dt occurrence, and remains low for the next few hours (Figure 11). One notable difference is that while the 26 June 1998 BEAR event was detected on the ground in the post-midnight to dawn sector the 7 January 2015 was detected by the CARISMA array closer to local midnight. As with the previous event, we provide the (magnetic north-south) H-component magnetometer time series from selected CARISMA magnetometer stations in Supplementary Material Figure S2. Because

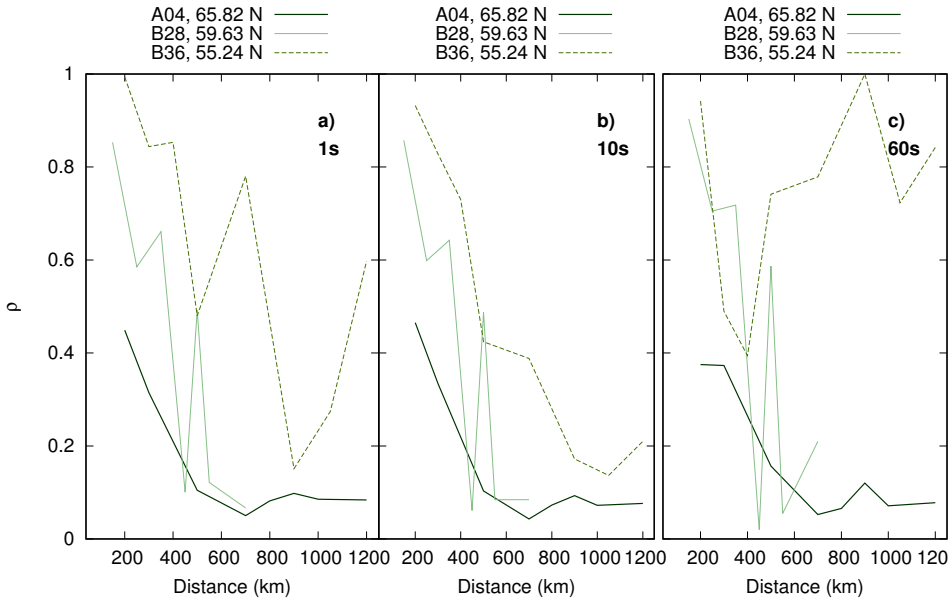

Figure 9. Vector correlation coefficients between measurements at three selected stations on the line of constant 105° E longitude (green) line of the BEAR array (A04, B28 and B36) with other stations on that line, between 1:00 and 5:00 UTC; and using magnetic data with a) a two second sampling rate, b) a ten second sampling rate, and c) a one minute sampling rate.

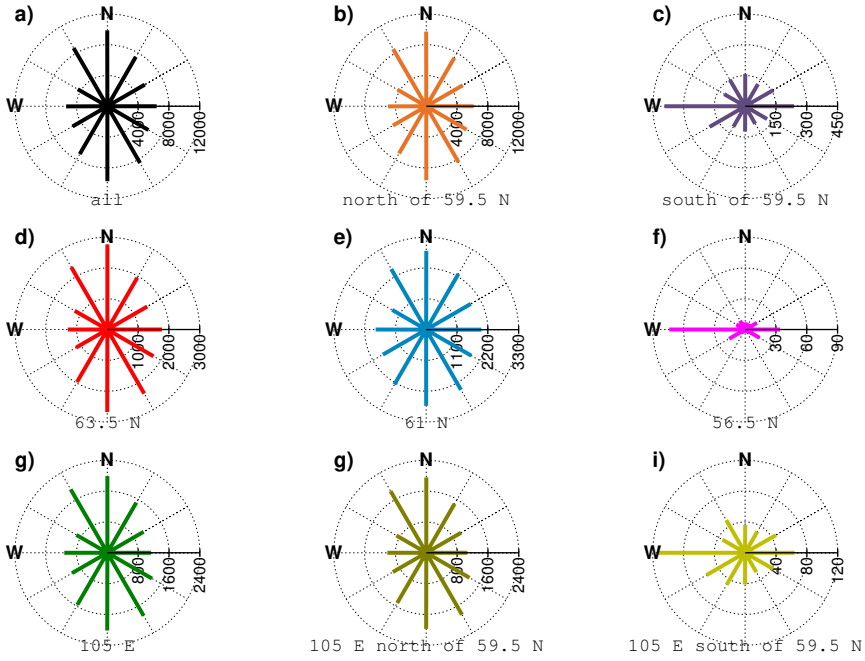

Figure 10. Angular polarisation occurrence of total number of $dB_H/dt > 1$nT/s, using 1s data, measured between 1:00 and 5:00 UTC at BEAR, for various groups of stations.

of the smaller number of stations, and the fact that they are all situated in Canada or the northern United States, we did not perform a separate analysis of northern and southern stations, as with BEAR. But we did group several stations along three lines of constant geomagnetic latitude or longitude, as shown in Figure 2. as with the BEAR event, stations along the southern (blue) line had fewer counts of $dB_H/dt > 1\text{nT/s}$ compared to stations along the northern (red) line. It is noteworthy that the occurrence peak in the south (blue line) occurred between 11:00 and 12:00 UTC, while the peak in the north (red line) had occurred earlier between 9:00 and 10:00 UTC. After 11:00 UTC, there was more activity observed in the blue line than in the red one. Figure 12 shows the occurrence rates of dB_H/dt as a function of threshold for the CARISMA groups of stations using 1s data. As in the BEAR case, there again appears a steepening of the slopes for the southern stations compared to the northern ones. The same result is again obtained using one minute cadence data. The resulting lines are again almost log-normal, with slightly higher curvature than the ones from the BEAR case, perhaps as a result of the lower count statistics. As in Figure 7 for the previous event, here we again show polar maps of magnetic perturbation vectors from SuperMAG for this event in Figure 13 for three selected times within the period of high dB_H/dt activity. Although there was no visual coverage of the auroral oval available from space at this time, we can see a similar ordering of dB_H/dt vectors within the same latitude range.

In Figure 14 we again show values of ρ plotted as a function of station separation distance. Because of the larger distances between the CARISMA stations, we cannot resolve distances below the 250 km bin. However, we can still see an indication of a decrease in coherence up to distances of around 500 km, after which the vector correlation flattens out near zero at larger scales. Interestingly, when we reduce our sampling rate to one minute, the correlation coefficients increase for all separation distances. This was also the case in Figure 8 but is more obvious here. This is probably because very localized $d\mathbf{B}_H/dt$ spikes are smoothed out when down-sampling the data. As with BEAR, we have also considered the correlations between three individual stations along a line of constant longitude, with all other stations at that longitude, with results shown in Figure 15. Consistent with the BEAR results, only the lowest latitude station shows appreciable magnetic correlation with other stations nearby. The median angles of $d\mathbf{B}_H/dt$ vectors at CARISMA, shown in Figure 16, are more homogeneous at all four different groups of stations than was the case for the BEAR event. This may be an effect of dif-

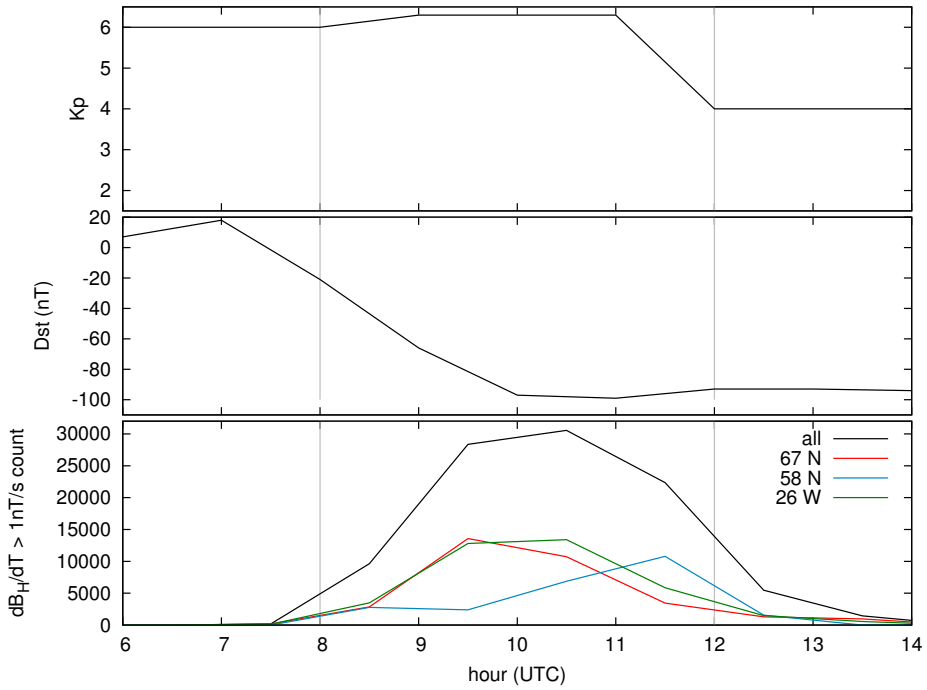

Figure 11. Kp (top), Dst (middle), and dB_H/dt counts per hour (bottom), on 7 January 2015 with the CARISMA array. Grey vertical lines show the time span of data used for analysis. Coloured lines in the bottom panel correspond to different subsets of stations, as shown in Figure 2.

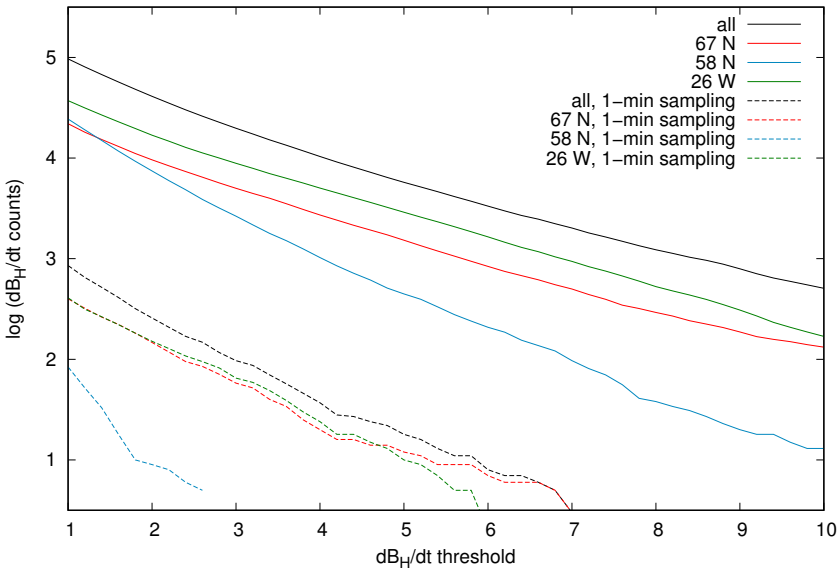

Figure 12. Occurrence distribution of dB_H/dt as a function of threshold (units of nT/s), using data from 01:00 to 5:00 UTC on 7 January 2015, for the CARISMA array; for all stations (black line), and along three lines of constant magnetic latitude or longitude (red, blue, and green lines). The short dashed lines show measurements with a one minute sampling rate.

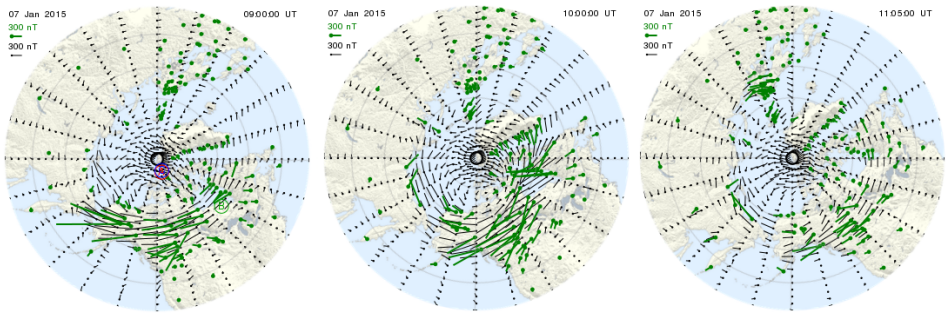

Figure 13. Polar maps from SuperMAG for the 7 January 2015 event. Three snapshots are shown, for 9:00 UTC, 10:00 UTC, and 11:05 UTC.

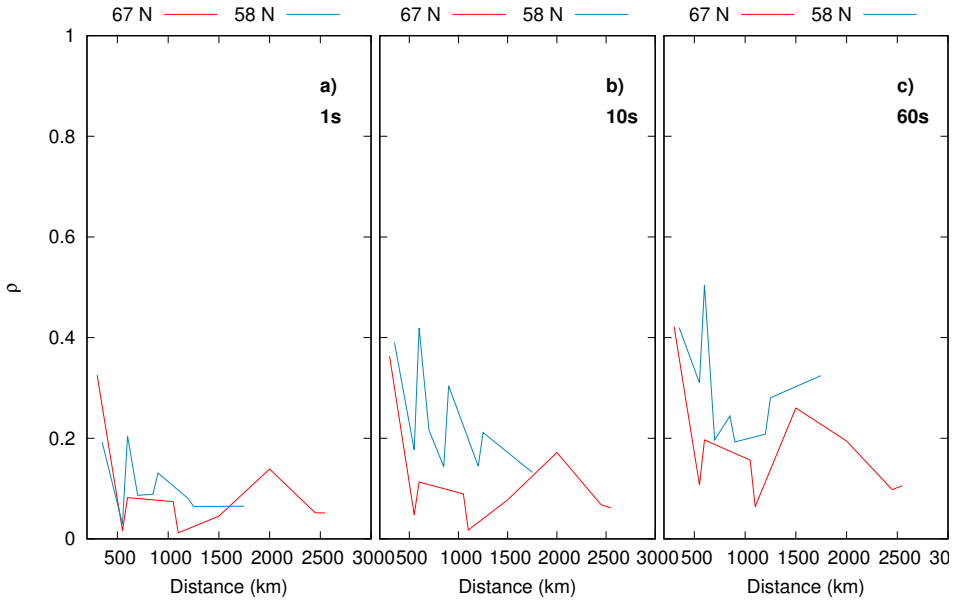

Figure 14. Vector correlation coefficients, used to compare the similarity of concurrent dB_H/dt vectors at different inter-station separation distances along two lines of constant latitude at 67 degrees N (red) and 58 degrees N (blue), between 8:00 and 12:00 UTC at CARISMA; and with a) a one second sampling rate, b) a ten second sampling rate, and c) a one minute sampling rate.

ferences between the magnetic disturbances for the two substorm events, at slightly different MLT, or due to the lack of a group of stations in CARISMA at sufficiently low latitude (cf. the magenta line for BEAR).

4 Discussion

Based on the vector inter-station GMC correlations presented here, spatial correlations range in scale from 100-500 km - the shortest correlation lengths occurring at higher latitudes and in proximity to the auroral zone. Current FERC guidelines mandate the use of spatially-averaged data in 500 km x 500 km regions, and do not take into account the effect of latitude on their measurements. Based on the GMD correlation length scales we report here, we conclude that these current FERC guidelines can be prone to under-reporting the intensity of localized GMD activity. Most areas of high population density and high economic activity lie at low latitudes, below the auroral zone, and would thus be well served by a 500 km magnetometer spacing under normal geomagnetic con-

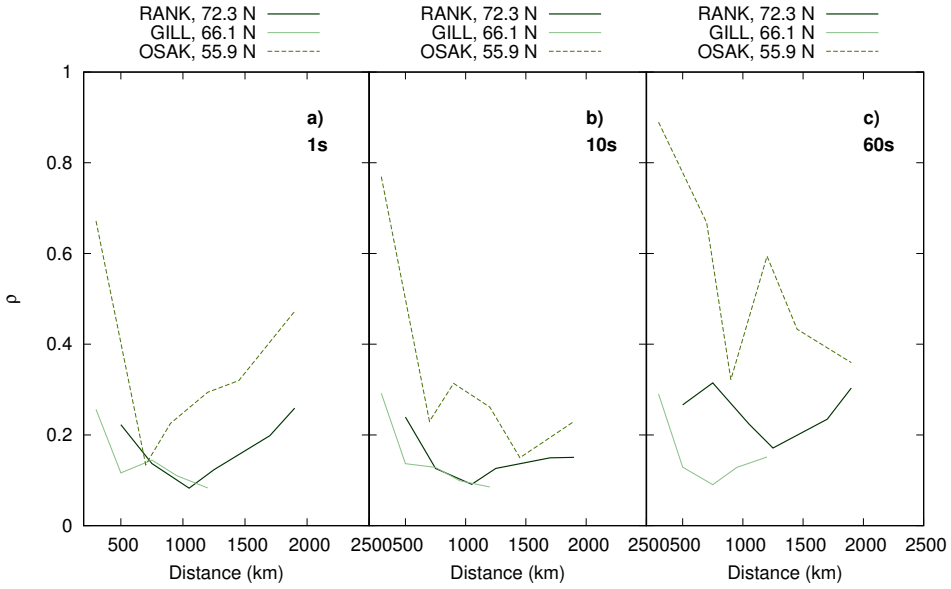

Figure 15. Vector correlation coefficients between measurements at three specific stations, RANK, GILL, and OSAK, on the 26 W (green) line of constant longitude at CARISMA and all other stations on that line, between 8:00 and 12:00 UTC; with a) a two second sampling rate, b) a ten second sampling rate, and c) a one minute sampling rate.

ditions. However, intense magnetic storms will push the auroral oval equatorward requiring a higher spatial resolution magnetic monitoring in order to properly characterise the GMD-related GIC risk. Overall, our results show that GMD tend to be very coherent at distances of $\sim$ 100 km, as expected since this corresponds to the approximate height of the E region of the ionosphere which carries the ionospheric currents driving the GMD. Based on our results, a station separation of $\sim$ 200 km would seem to be more appropriate for more accurately capturing the small scale variability of the GMD. A one-minute sampling rate appears does appear to provide slightly higher coherence of measurements for all distances, but not high enough to make up for the variability at higher latitudes. Moreover, one minute cadence data is too slow to fully capture the timescales of GMD which are important for GICs, and in our view monitoring at 1s cadence is preferred.

A similar comparison of the spatial scales of GMD in North America was undertaken by (Butala et al., 2017), including some of the CARISMA stations, but mostly focusing on lower latitudes. By obtaining cross correlations between north and east magnetic measurements, these authors found that variances can only be accurately modelled

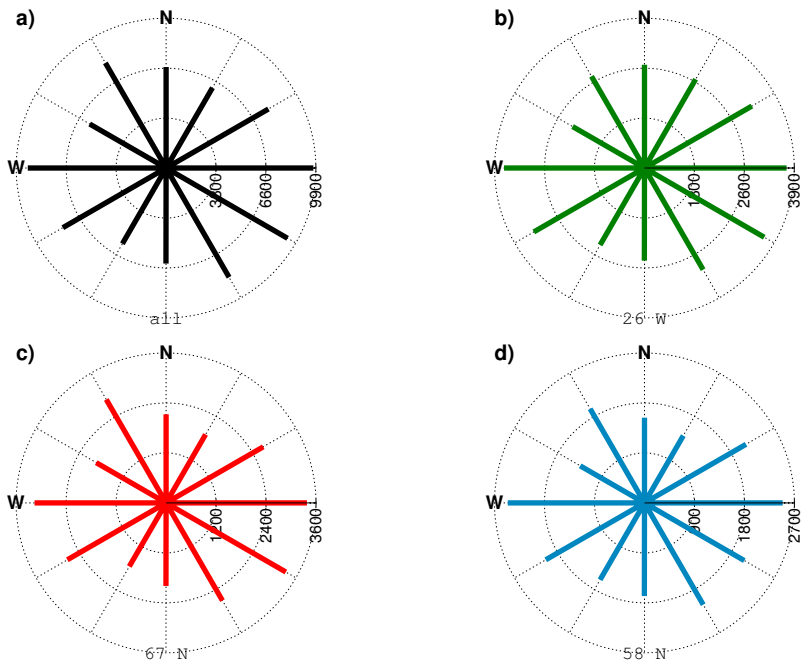

Figure 16. Occurrence of polarisations of events with $dB_H/dt > 1$nT/s, measured between 8:00 and 12:00 UTC at CARISMA using 1s data, for various groups of stations. (a) All, (b) at 26 degrees W longitude, (c) at 67 degrees N latitude (higher latitude), and (d) at 58 degrees N latitude (lower latitude).

at short distances from each magnetometer, which agrees with our results. However, they were limited to a sampling rate of 60s and to geomagnetic latitudes below 58° N, and as we have demonstrated here the correlation lengths can be different at different latitudes. Dimmock et al. (2020) also looked into the regional variability of dB/dt in Scandinavia using 10s resolution data. They employed a different approach, comparing dB_H/dt from single stations to the average derived from other sets of stations. By assuming that those dB_H/dt variations induce currents on a grid of transmission lines, they found that even on scales of $\sim$ 200 km there was a regional variability of up to 60% in peak voltages compared to the assumption of a uniform magnetic disturbance field. A spatial scale of 200 km was also proposed by EPRI (2020), after an examination of the statistics of localized geoelectric field enhancements in Canada and Scandinavia.

The two storms we considered here, while otherwise similar according to their geomagnetic indices, represent geomagnetic disturbances centered on the local dawn and midnight sectors, respectively. The midnight activity is characteristic of Disturbance Polar 1 surface magnetic field perturbations, brought upon by the substorm current wedge during the sustorm's expansion phase. Similar perturbations at dawn would be more indicative of activity on the flank of the magnetosphere and most likely related to global convection. This highlights the importance of considering multiple mechanisms when modelling the risk of GICs (e.g., Freeman et al., 2019). Our method can be expanded to take into account multiple other storms under different geomagnetic conditions, drawing on the decades of CARISMA observations, including for the analysis of the occurrence distributions and statistics of the magnitudes of the worst case GMD, and that will be the focus of future work.

5 Conclusions

From an investigation of ground magnetic field measurements for two similar periods of geomagnetic activity during geomagnetic storms as observed by two magnetometer arrays with elements spanning different spatial scales (BEAR in Scandinavia and CARISMA in Canada; in the local pre-dawn to dawn, and local midnight sectors, respectively) we have found the following:

- Occurrence distributions of $d\mathbf{B}_H/dt$ are log-normal (in the case of BEAR) or close to log-normal (in the case of CARISMA) for magnitudes up to around 10nT/s, where the statistics become sparse;
- For the events studied here, there is evidence that there is a sharp gradient in these occurrence distributions above and below 60 degrees magnetic latitude;
- The locations of regions of high $d\mathbf{B}_H/dt$ appear to be closely related to the location of the auroral oval;
- The spatial scale of high $d\mathbf{B}_H/dt$ vector correlation between stations of varying separation is shorter at higher latitudes; it remains high for distances exceeding 400 km when only considering stations at latitudes lower than the auroral oval;
- The magnitudes of $d\mathbf{B}_H/dt$ statistically decrease with decreasing latitude. The GMD also have larger magnitudes in nT/s when measured at 1s cadence, rather than at 10s or 1 minute cadence, indicative of the short-scale temporal variability of the GMD;
- In general, there is no directional preference for $d\mathbf{B}_H/dt$ vector polarisation (when $d\mathbf{B}_H/dt > 1$nT/s) for higher latitudes (within the auroral oval); there is some evidence for a preference for East-West GMD polarisation at sub-auroral latitudes;
- Since the auroral oval is pushed southward during intense magnetic storms, a higher magnetometer station density is required to accurately assess the ground impact of GMD across all latitudes at all times. Therefore a station separation of ~ 200 km is recommended as being optimal as a general requirement for GMD monitoring for GIC applications.

Acknowledgments

SD was supported by the Canadian Space Agency through the Geospace Observatory (GO) Canada program. IRM is supported by a Discovery Grant from Canadian NSERC. CARISMA is operated by the University of Alberta, funded by the Canadian Space Agency. For the Polar VIS Earth Camera images we gratefully acknowledge the Polar VIS Earth Camera team, PI Prof. Louis A Frank. We acknowledge use of NASA/GSFC's Space Physics Data Facility's OMNIWeb service, and OMNI data. The data from BEAR used in this paper are available at: https://osf.io/jcv3d/?view_only=46769e5350ac459c89c96c25f92d0cd3 CARISMA magnetometer data are available at: www.carisma.ca.

References

Bolduc, L., Langlois, P., Boteler, D., & Pirjola, R. (1998, October). A study of geoelectromagnetic disturbances in Quebec, 1. general results. *IEEE Transactions on Power Delivery*, *13*(4).

Boteler, D. H., & Pirjola, R. J. (2017). Modeling geomagnetically induced currents. *Space Weather*, *15*(1), 258–276. Retrieved from `http://dx.doi.org/10.1002/2016SW001499` (2016SW001499) doi: 10.1002/2016SW001499

Boteler, D. H., Pirjola, R. J., & Nevanlinna, H. (1998). The effects of geomagnetic disturbances on electrical systems at the earth's surface. *Advances in Space Research*, *22*, 17-27. doi: 10.1016/S0273-1177(97)01096-X

Butala, M. D., Kazerooni, M., Makela, J. J., Kamalabadi, F., Gannon, J. L., Zhu, H., & Overbye, T. J. (2017, October). Modeling Geomagnetically Induced Currents From Magnetometer Measurements: Spatial Scale Assessed With Reference Measurements. *Space Weather*, *15*, 1357-1372. doi: 10.1002/2017SW001602

Coles, R. L., & Boteler, D. H. (1993). *Geomagnetic induced currents: assessment of geomagnetic hazard* (Report). GSC Open File 2635.

Coles, R. L., Thompson, K., & Jansen van Beek, G. (1992). A comparison between the rate of change of the geomagnetic field and geomagnetically induced currents in a power transmission system..

Dimmock, A. P., Rosenqvist, L., Welling, D. T., Viljanen, A., Honkonen, I., Boynton, R. J., & Yordanova, E. (2020). On the regional variability of db/dt and its significance to gic. *Space Weather*, *18*(8), e2020SW002497. Retrieved from `https://agupubs.onlinelibrary.wiley.com/doi/abs/10.1029/2020SW002497` (e2020SW002497 10.1029/2020SW002497) doi: https://doi.org/10.1029/2020SW002497

EPRI. (2020). *Furthering the understanding of the characteristics and scales of geoelectric field* (Report No. 3002017900). EPRI, Palo Alto, CA.

Frank, L. A., Sigwarth, J. B., Craven, J. D., Cravens, J. P., Dolan, J. S., Dvorsky, M. R., ... Muller, D. W. (1995, February). The Visible Imaging System (VIS) for the Polar Spacecraft. *Space Sci. Rev.*, *71*(1-4), 297-328. doi: 10.1007/BF00751334

Freeman, M. P., Forsyth, C., & Rae, I. J. (2019, June). The Influence of Sub-

storms on Extreme Rates of Change of the Surface Horizontal Magnetic Field in the United Kingdom. *Space Weather*, *17*(6), 827-844. doi: 10.1029/2018SW002148

Gjerloev, J. W. (2009, July). A Global Ground-Based Magnetometer Initiative. *EOS Transactions*, *90*, 230-231. doi: 10.1029/2009EO270002

Gjerloev, J. W. (2012, September). The SuperMAG data processing technique. *Journal of Geophysical Research (Space Physics)*, *117*, A09213. doi: 10.1029/2012JA017683

Hanson, B., Klink, K., Matsuura, K., Robeson, S., & Willmott, C. (1992, 03). Vector correlation: Review, exposition, and geographic application. *Annals of The Association of American Geographers - ANN ASSN AMER GEOGR*, *82*, 103-116. doi: 10.1111/j.1467-8306.1992.tb01900.x

Heyns, M. J., Lotz, S. I., & Gaunt, C. T. (2021). Geomagnetic pulsations driving geomagnetically induced currents. *Space Weather*, *19*(2), e2020SW002557. Retrieved from `https://agupubs.onlinelibrary.wiley.com/doi/abs/10.1029/2020SW002557` (e2020SW002557 10.1029/2020SW002557) doi: https://doi.org/10.1029/2020SW002557

Hjelt, S. E., & Daly, S. (1996). SVEKALAPKO, Evolution of Palaeoproterozoic and Archaean Lithosphere..

Huttunen, K. E. J., Kilpua, S. P., Pulkkinen, A., Viljanen, A., & Tanskanen, E. (2008). Solar wind drivers of large geomagnetically induced currents during the solar cycle 23. *Space Weather*, *6*(10). Retrieved from `https://agupubs.onlinelibrary.wiley.com/doi/abs/10.1029/2007SW000374` doi: https://doi.org/10.1029/2007SW000374

Kataoka, R., & Pulkkinen, A. (2008). Geomagnetically induced currents during intense storms driven by coronal mass ejections and corotating interacting regions. *Journal of Geophysical Research: Space Physics*, *113*(A3). Retrieved from `https://agupubs.onlinelibrary.wiley.com/doi/abs/10.1029/2007JA012487` doi: https://doi.org/10.1029/2007JA012487

Lanzerotti, L. J. (1979, August). Geomagnetic influences on man-made systems. *Journal of Atmospheric and Terrestrial Physics*, *41*, 787-796. doi: 10.1016/0021-9169(79)90125-9

Lysak, R. L. (1991). Feedback instability of the ionospheric resonant cavity. *Journal*

of Geophysical Research: Space Physics, *96*(A2), 1553-1568. Retrieved from https://agupubs.onlinelibrary.wiley.com/doi/abs/10.1029/90JA02154 doi: https://doi.org/10.1029/90JA02154

Mäkinen, T. (1992). Geomagnetically induced currents in the Finnish power transmission system. *Finnish Meteorological Institute Geophysical Publications*(32), 101.

Mann, I. R., Milling, D. K., Rae, I. J., Ozeke, L. G., Kale, A., Kale, Z. C., ... Singer, H. J. (2008, December). The Upgraded CARISMA Magnetometer Array in the THEMIS Era. *Space Science Reviews*, *141*, 413-451. doi: 10.1007/s11214-008-9457-6

Marshall, R. A., Waters, C. L., & Sciffer, M. D. (2010, May). Spectral analysis of pipe-to-soil potentials with variations of the Earth's magnetic field in the Australian region. *Space Weather*, *8*, 05002. doi: 10.1029/2009SW000553

Molinski, T. S. (2002, November). Why utilities respect geomagnetically induced currents. *Journal of Atmospheric and Solar-Terrestrial Physics*, *64*, 1765-1778. doi: 10.1016/S1364-6826(02)00126-8

NERC. (2012, February). 2012 Special Reliability Assessment Interim Report: Effects of Geomagnetic Disturbances on the Bulk Power System.

Pulkkinen, A., Bernabeu, E., Eichner, J., Viljanen, A., & Ngwira, C. (2015, June). Regional-scale high-latitude extreme geoelectric fields pertaining to geomagnetically induced currents. *Earth, Planets, and Space*, *67*, 93. doi: 10.1186/s40623-015-0255-6

Pulkkinen, A., Klimas, A., Vassiliadis, D., Uritsky, V., & Tanskanen, E. (2006, March). Spatiotemporal scaling properties of the ground geomagnetic field variations. *Journal of Geophysical Research (Space Physics)*, *111*, A03305. doi: 10.1029/2005JA011294

Rodger, C. J., Mac Manus, D. H., Dalzell, M., Thomson, A. W. P., Clarke, E., Petersen, T., ... Divett, T. (2017, November). Long-Term Geomagnetically Induced Current Observations From New Zealand: Peak Current Estimates for Extreme Geomagnetic Storms. *Space Weather*, *15*, 1447-1460. doi: 10.1002/2017SW001691

Thomson, A. W. P., Dawson, E. B., & Reay, S. J. (2011, October). Quantifying extreme behavior in geomagnetic activity. *Space Weather*, *9*, S10001. doi: 10

.1029/2011SW000696

United States of America Federal Energy Regulatory Commission. (2016, September). Reliability Standard for Transmission System Planned Performance for Geomagnetic Disturbance Events, Order No. 830.

Viljanen, A. (1998, October). Relations of geomagnetically induced currents and local geomagnetic variations. *IEEE Transactions on Power Delivery*, *13*(4).

Viljanen, A. (2012). 3B. Description of the magnetospheric/ionospheric sources. In A. D. Chave & A. G. Jones (Eds.), *The magnetotelluric method: Theory and practice.* Cambridge University Press.

Viljanen, A., Nevanlinna, H., Pajunpää, K., & Pulkkinen, A. (2001, September). Time derivative of the horizontal geomagnetic field as an activity indicator. *Annales Geophysicae*, *19*, 1107-1118. doi: 10.5194/angeo-19-1107-2001

Viljanen, A., Tanskanen, E. I., & Pulkkinen, A. (2006). Relation between substorm characteristics and rapid temporal variations of the ground magnetic field. *Annales Geophysicae*, *24*(2), 725–733. Retrieved from `https://angeo.copernicus.org/articles/24/725/2006/` doi: 10.5194/angeo-24-725-2006

Waters, C. L., Gjerloev, J. W., Dupont, M., & Barnes, R. J. (2015). Global maps of ground magnetometer data. *Journal of Geophysical Research: Space Physics*, *120*(11), 9651-9660. Retrieved from `https://agupubs.onlinelibrary.wiley.com/doi/abs/10.1002/2015JA021596` doi: https://doi.org/10.1002/2015JA021596

Woodroffe, J. R., Morley, S. K., Jordanova, V. K., Henderson, M. G., Cowee, M. M., & Gjerloev, J. G. (2016, September). The latitudinal variation of geoelectromagnetic disturbances during large (Dst≤-100 nT) geomagnetic storms. *Space Weather*, *14*, 668-681. doi: 10.1002/2016SW001376